Spin Density Wave versus Fractional Magnetization Plateau in a Triangular Antiferromagnet

L. Facheris,[1,*] K. Yu. Povarov,[1] S. D. Nabi,[1] D. G. Mazzone,[2] J. Lass,[2,3] B. Roessli,[2] E. Ressouche,[4] Z. Yan,[1] S. Gvasaliya,[1] and A. Zheludev[1,†]

[1]*Laboratory for Solid State Physics, ETH Zürich, 8093 Zürich, Switzerland*
[2]*Laboratory for Neutron Scattering and Imaging, Paul Scherrer Institute, CH-5232 Villigen, Switzerland*
[3]*Department of Physics, Technical University of Denmark, DK-2800 Kongens Lyngby, Denmark*
[4]*Université Grenoble Alpes, CEA, IRIG, MEM, MDN, 38000 Grenoble, France*

(Received 22 April 2022; accepted 19 July 2022; published 16 August 2022)

We report an excellent realization of the highly nonclassical incommensurate spin-density wave (SDW) state in the quantum frustrated antiferromagnetic insulator Cs_2CoBr_4. In contrast to the well-known Ising spin chain case, here the SDW is stabilized by virtue of competing planar in-chain anisotropies and frustrated interchain exchange. Adjacent to the SDW phase is a broad $m = 1/3$ magnetization plateau that can be seen as a commensurate locking of the SDW state into the up-up-down (UUD) spin structure. This represents the first example of the long-sought SDW–UUD transition in triangular-type quantum magnets.

DOI: 10.1103/PhysRevLett.129.087201

Of the various magnetically ordered phases of insulators, the spin-density wave (SDW) is perhaps the least classical one [1,2]. While easily envisioned in metals where the spin carriers are itinerant [3], it cannot exist in classical models with localized spins of given magnitude at each site. Nevertheless, there are several purely quantum-mechanical routes to realizing SDW states in insulators. To a greater or lesser extent they are all based on the Tomonaga-Luttinger spin liquid (TLSL) properties of the $S = 1/2$ quantum spin chain with antiferromagnetic (AF) exchange interactions J. In applied magnetic fields, a single chain develops incommensurate spin correlations in the longitudinal channel [4,5]. In most cases though, the transverse commensurate correlations dominate, eventually resulting in transverse AF or helical long-range order in coupled chains. To create a SDW, one needs to somehow boost the longitudinal correlations in each chain or to ensure that they are favored by interchain interactions. The first approach, realized in materials like $BaCo_2V_2O_8$ [6,7] and $SrCo_2V_2O_8$ [8], is to simply endue the chains with Ising-type anisotropy. Another route, realized quite recently [9,10], is to impose Ising anisotropy on *interchain* interactions J'. This is arguably the case of $YbAlO_3$ [11,12]. The third route to a SDW state exploits *frustrated* zig-zag interchain bonds J' in the so-called "distorted triangular lattice" geometry. Commensurate transverse TLSL correlations in each chain become completely decoupled at the mean field (MF) level; incommensurate longitudinal ones are not, and are thus the ones to order in 3D. In this model theory predicts a SDW phase in a very wide range of J'/J ratios [13–15]. A very special feature of this mechanism is the SDW "locking" to a commensurate wave vector producing a $m = 1/3$ up-up-down (UUD) magnetization plateau state. The latter persists even if $J = J'$, where no chains can be identified, and even in the fully isotropic case [16]. It thus establishes an important link between 1D TLSL and 2D triangular lattice physics. To date, this connection remains poorly understood experimentally, for lack of a suitable model system.

In the present Letter we demonstrate the existence of an incommensurate SDW state and its locking into a UUD phase in the triangular-lattice magnet Cs_2CoBr_4 [17]. Both phases are well pronounced and occupy nearly a quarter of the phase diagram each. The mechanism behind this phenomenon is likely to be a blend of the three "routes to SDW" described above.

Our target material Cs_2CoBr_4 crystallizes in the orthorhombic P_{nma} structure, same as that of Cs_2CuCl_4 [18,19], Cs_2CuBr_4 [20], and Cs_2CoCl_4 [21–23]. The magnetic $3d$ ions (four per unit cell) are arranged in triangular-patterned layers in the bc plane. The two Cu-based compounds mentioned above are straightforward $S = 1/2$ Heisenberg $J - J'$ model magnets [13]. The physics of Cs_2CoCl_4 and our material is more complicated. The Co^{2+} magnetic ions sit in a low-symmetry distorted tetrahedral environment, thus their orbital momentum is quenched. Their magnetism is described in the language of $S = 3/2$ spins dominated by crystal-field effects. The latter reduce the magnetism to *pseudospin* $\tilde{S} = 1/2$ degrees of freedom at low temperatures. In the pseudospin representation the interactions are strongly modified, yielding a nearly XY-type coupling. The effect is strongest for intrachain J interactions along the $\boldsymbol{b}$ axis. These anisotropic interactions are mostly a crystal

field effect, in contrast to more symmetric situations where anisotropic interactions arise from direct spin-orbit entanglement [24,25]. In Cs_2CoCl_4 the zig-zag interchain interactions J' are negligible, making the material a nearly ideal XY chain [23,26]. A distinctive feature of Cs_2CoBr_4 is that J' is much stronger and comparable to J [17]. This creates a novel type of frustration, in addition to the already-present geometric frustration of J'. The crystal structure dictates mutually perpendicular directions of the planar anisotropy in neighboring chains. The $\boldsymbol{b}$ direction is shared by both planes. In this way two easy-plane anisotropies conspire to effectively produce an easy-$\boldsymbol{b}$-axis anisotropy for the pseudospins.

Below $T_N = 1.3$ K, as a function of magnetic field applied along the $\boldsymbol{b}$ direction, Cs_2CoBr_4 goes through a sequence of five magnetic phases [17]. The first and the third phases in increasing fields are magnetization plateaux, with pseudospin magnetization $\tilde{m} \simeq 0$ and $1/3$, correspondingly. In this study we use neutron diffraction to unambiguously identify these states as the antiferromagnetic stripe phase (AF) with propagation vector $\mathbf{Q} = (0, 1/2, 1/2)$, and UUD phase with $\mathbf{Q} = (0, 1/3, 0)$. The intermediate second magnetic state turns out to be a longitudinal incommensurate SDW with propagation vector $\mathbf{Q} = (0, \xi, 0)$. The experiment was performed on the CEA-CRG D23 lifting-counter diffractometer at ILL (Grenoble, France). The 24.90(4) mg single crystal of Cs_2CoBr_4 was mounted on the cold finger of a dilution refrigerator $T \lesssim 0.1$ K in a vertical 6 T cryomagnet, with $\mathbf{H}\|\boldsymbol{b}$ and ac being in the horizontal scattering plane. This setting allowed us to cover $|h| \leq 6$, $-1 \leq k \leq 0$, and $|l| \leq 7$ r.l.u. portion of the (h, k, l) reciprocal space with $\lambda = 2.36$ Å neutrons (PG002), in which the Bragg peaks of the types described above were collected in magnetic fields of 0, 2.2, and 3.2 T correspondingly. The symmetry-based group theory analysis and model refinement (using SARAh [27] and FullProf Suite [28,29]) suggest the collinear configurations shown in Fig. 1(a) to be the optimal solutions with R factors 7.1%, 14.8%, and 11% for AF, SDW, and UUD, correspondingly. The field dependencies of magnetic order parameters $M_{\mathbf{Q}}$ associated with each phase (*modulation amplitudes* at the given propagation vectors $\mathbf{Q}$) are shown in Fig. 1(c). For AF and UUD phases, the Bragg peak intensity was measured by counting at fixed $\mathbf{Q}$ versus field. For the SDW phase, the peak positions and intensities were extracted from broad k scans at eight field values [28]. The AF order parameter disappears above the discontinuous AF-SDW transition at 1.5 T in agreement with thermodynamics [17]. The apparent residual intensity at $(0, -1/2, 3/2)$ in Fig. 1(c) is due to a simple background model [28]. In contrast, the SDW-UUD transition seems to be a quintessential incommensurate-commensurate locking, with rather insignificant jump in the spin modulation depth. The residual intensity of $(0, -1/3, 1)$ below 2.8 T is due to the poor resolution along the vertical k direction.

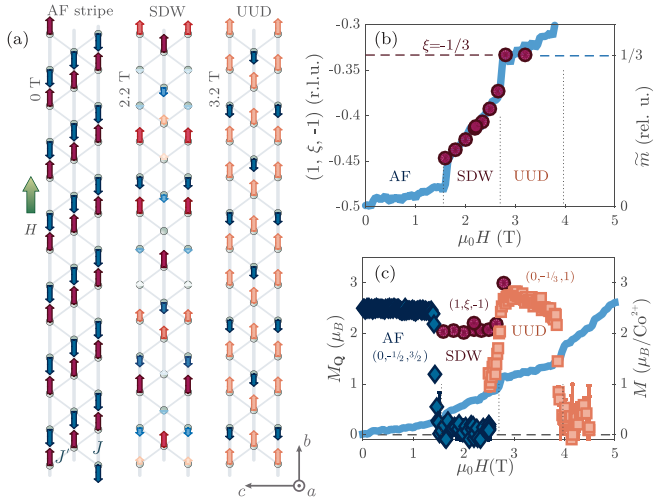

FIG. 1. Diffraction results for Cs_2CoBr_4, $\mathbf{H}\|\boldsymbol{b}$. (a) AF-stripe, SDW, and UUD phases shown in pseudospin representation. Color denotes the relative depth of on-site modulation. Exchange couplings J and J' are also indicated. (b) Points: incommensurate Bragg peak position of the SDW phase versus field. The blue line shows the "pseudospin" relative magnetization [17]. (c) Magnetic order parameter (modulation amplitude) $M_{\mathbf{Q}}$ vs field for AF (diamonds), SDW (circles), and UUD (squares) phases. The corresponding wave vectors of actual measurement are also indicated. The blue line is the magnetization curve $M(H)$ [17]. All measurements are performed at $T \lesssim 0.1$ K.

The $M_{\mathbf{Q}}$ extracted from the broad k scan at 2.8 T inside the UUD phase agrees well with the more precise UUD dataset.

The field dependence of the SDW propagation vector $(0, \xi, 0)$ was extracted from the same k scans mentioned above. The result is plotted in Fig. 1(b). Remarkably, the propagation vector closely follows the pseudospin relative magnetization [17]:

$$|\xi| = 1/2 - \tilde{m}/2. \tag{1}$$

Such behavior is typical of longitudinal incommensurate correlations specific to $S = 1/2$ chains. In the TLSL framework this incommensurability corresponds to a nesting vector that spans the Fermi sea of *fractionalized spinon quasiparticles* [1]: $\xi = 2k_F$. This picture may provide the basic idea for understanding the physics of Cs_2CoBr_4, but the analogy is difficult to extend beyond Eq. (1). The actual field dependence of magnetization shown in Fig. 1(b) is entirely different from that of an XXZ chain in longitudinal field [1,6,7].

Equation (1) also holds for coupled-chain models, the Heisenberg J-J' model in particular [13–15]. Similar types of field dependencies were previously also observed in the Ising chains [6–8], or Ising-coupled Heisenberg chains [11,12]. A very narrow "elliptical spiral" phase with linear incommensuration-field dependence was also reported for the structurally similar Heisenberg J-J' magnet Cs_2CuCl_4 [18]. In all

these cases, however, the UUD phase at $\xi = 1/3$ is either absent altogether (Ising chains), or is very narrow compared to the SDW state ($YbAlO_3$). In the latter case, theory does not predict any plateau for the corresponding Ising-coupled Heisenberg chain model [9,10]. It has been proposed that the commensurate-incommensurate locking in $YbAlO_3$ might be the consequence of, e.g., additional small interactions [12]. The coexistence of a magnetization-scaled SDW and well-defined plateau is unique for Cs_2CoBr_4.

To get more insight into the mechanism of the AF-SDW-UUD sequence of transitions, we have measured the magnetic excitation spectra at zero field (AF) and at 1.8 T (SDW). The experiment was performed on the new CAMEA spectrometer at PSI (Switzerland) [30]. The $m = 1.16$ g crystal of Cs_2CoBr_4 was mounted on the cold finger of a dilution refrigerator with bc in the scattering plane. A 1.8 T horizontal magnet was used, with the direction of the field set along $\boldsymbol{b}$. The unique combination of the multiplexing capabilities of CAMEA, the "continuous angle" data acquisition mode, and the open geometry of this horizontal magnet allowed us to obtain a detailed neutron scattering intensity dataset vs $(k, l, \hbar\omega)$ in both AF and SDW states. Two measurement series were performed at each field, with $E_i = 5.1$ and $E_i = 3.6$ meV, for higher coverage and higher resolution correspondingly (~0.16 meV FWHM). The projections from the cumulative datasets for AF ($\mu_0 H = 0$) and SDW ($\mu_0 H = 1.8$ T) phases are shown in Fig. 2. In zero field the spectrum is gapped ($\Delta \simeq 0.35$ meV) and mostly dispersive along the $\boldsymbol{b}$ direction, with the bandwidth approaching 0.7 meV. In addition to the pronounced magnonlike excitation at low energy, a continuum with a sharp upper boundary is clearly visible. At higher energies, $E_{CF} = 2.1(1)$ meV, we observe a nondispersive level (see [28] for extra data), that can be understood as $|1/2\rangle \rightarrow |3/2\rangle$ transition of cobalt $S = 3/2$ at energy $2D$. This gives $D = 12.2(6)$ K, in good agreement with the susceptibility-based estimate of 14(1) K reported earlier [17].

The strength of J' interactions is key to understanding the physics of Cs_2CoBr_4. As Fig. 3 shows, the bandwidth along the $\mathbf{c}$ axis is only about 0.1 meV. This, however, is not a sign of an insignificant J', but rather of geometric frustration in the zig-zag interchain coupling and of its predominant Ising nature. For a crude estimate we can rely on a simple spin wave theory (SWT) calculation (using the SpinW package [28,31]). The starting point is the Hamiltonian

$$\hat{\mathcal{H}} = \sum_{i,j} \sum_{\alpha=x,y,z} J_e^{\alpha\alpha} \hat{\tilde{S}}^{\alpha}_{i,2j} \hat{\tilde{S}}^{\alpha}_{i+1,2j} + J_o^{\alpha\alpha} \hat{\tilde{S}}^{\alpha}_{i,2j+1} \hat{\tilde{S}}^{\alpha}_{i+1,2j+1} + J'^{\alpha\alpha} \hat{\tilde{S}}^{\alpha}_{i,2j} [\hat{\tilde{S}}^{\alpha}_{i,2j+1} + \hat{\tilde{S}}^{\alpha}_{i,2j-1}], \quad (2)$$

with j and i enumerating the chains and sites within, and the diagonal exchange tensors being $J^{\alpha\alpha}_{e,o} = J(1, 1+\delta, 1-\Delta_{XY})$ and $J(1-\Delta_{XY}, 1+\delta, 1)$ for even and odd chains; $J'^{\alpha\alpha} = J'(1-\delta', 1, 1-\delta')$ for zig-zag bonds. Parameters $\Delta_{XY} = 0.75$ and $\delta' = 0.5$ are fixed from the basic pseudospin representation arguments [17,22]. This is

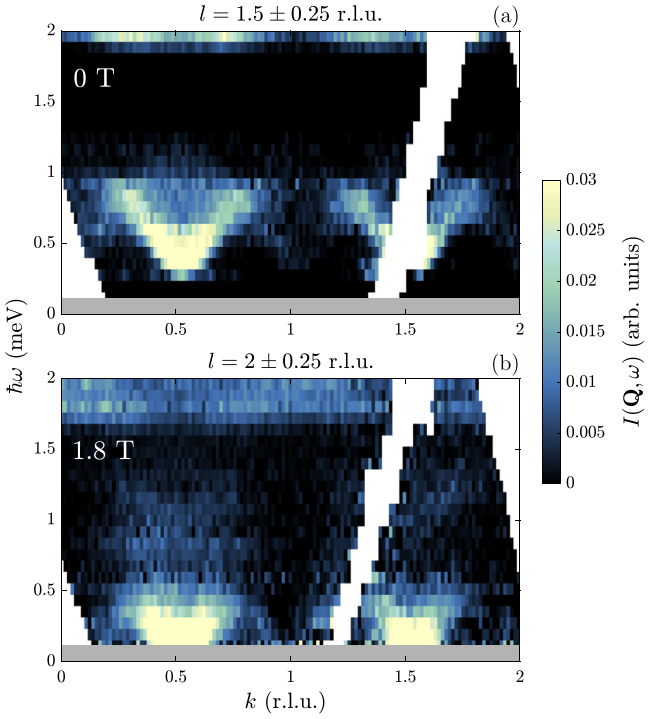

FIG. 2. Overview of magnetic excitations in Cs_2CoBr_4 at $T \lesssim 0.1$ K in (a) zero field and (b) 1.8 T. Color indicates the neutron scattering intensity proportional to the dynamic structure factor $\mathcal{S}(\mathbf{Q}, \omega)$. The data are integrated along $\mathbf{c}^*$ direction within the limits indicated. Background subtraction was performed as described in [28]. Gray areas mask regions where the incoherent scattering dominates over the signal.

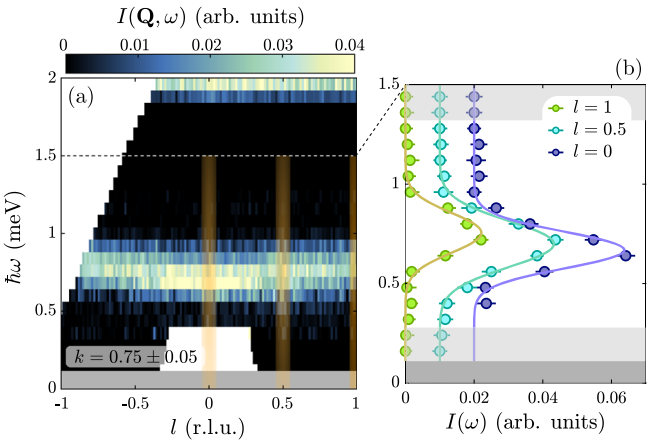

FIG. 3. (a) Dispersion along the $\mathbf{c}^*$ direction measured in Cs_2CoBr_4 at $T \lesssim 0.1$ K in zero field. The particular k value and integration range are indicated in the plot. (b) Intensity vs energy transfer cuts at different momenta, integrated in 0.05 r.l.u. along l [see orange stripes in (a)]. Dark gray areas mask the incoherent scattering, while light gray bands hide points excluded from the fit.

just a minor extension of the model presented earlier [17], which corresponds to $\delta = 0$. As discussed in the Supplemental Material, a good description of the main sharp spectral features is obtained with $J \simeq 0.8$ meV, $J' \simeq 0.35$ meV, and tiny additional Ising-type anisotropy $\delta = 0.1$ present on the main J bond. Since the semiclassical linear spin wave theory is ill defined for systems involving strong quantum fluctuations like Cs_2CoBr_4, these results are a good approximation only of the low-energy spectrum [28,32,33]. For this reason, we adopted an independent approach to estimate the ratio of J'/J: By using the Ising spin chain as the starting point, and then the random phase approximation, the bandwidth along and transverse to the chain direction can be obtained [28,34,35]. This approach also points to a significant $J'/J \gtrsim 0.4$ exchange ratio (see [28]). We conclude that in Cs_2CoBr_4 *the interchain coupling is almost half as strong as the in-chain one*. This is consistent with the observed spectrum being entirely different from that in weakly coupled Ising spin chains with a pronounced "Zeeman ladder" of spinonic bound states [36], such as in $BaCo_2V_2O_8$ [37].

We turn to the dynamics of the SDW phase. The corresponding dataset from CAMEA is actually quite unique, given the horizontal-field scattering geometry, the low energy scales, and the wide reciprocal-space coverage. The data collected at $\mu_0 H = 1.8$ T are visualized in Figs. 2(b) and 4. Compared to zero field, the spectrum measured in the SDW phase is much broader and clearly gapless. The latter agrees with the conclusions drawn from thermodynamic measurements [17]. As could be expected, the excitation energy goes to zero at the incommensurate $(0, \xi, 0)$ positions of the SDW where the corresponding Bragg peaks are located. However, there is one crucial difference with the single-chain TLSL spectrum of longitudinal excitations. In the latter, the spectrum is symmetric with respect to the $k = 1/2$ point. In Cs_2CoBr_4 it is not. The sign of ξ in Eq. (1) describing the Bragg peak and soft mode location corresponds to the parity of l for odd $k \sim 1/2$, but is reversed for $k \sim 3/2$. This "staggered" pattern of soft modes is once again dictated by the quasitriangular, rather than chainlike, nature of the underlying ionic lattice. Fig. 4(f) shows this clearly. The low-energy intensity is condensed around the side edges of the hexagonal zones. The low-energy excitations with linear dispersion emanate from the corresponding Bragg peaks. Their shape at higher energy transfer appears symmetric around $k = 1/2$, as Fig. 4(e) shows. The high energy part of the spectrum seems to be rather diffuse. We cannot identify any sharp modes above 0.4 meV. This may be due to the splitting and smearing of the zero-field spectrum by noncommuting magnetic fields, although the scenario with spinon complex continua, characteristic of longitudinal fluctuations in the TLSL phase [1], cannot be ruled out either. Moreover, the nondispersive level has now shifted to $E'_{\mathrm{CF}} \simeq 1.7(1)$ meV, in agreement with the expectations for

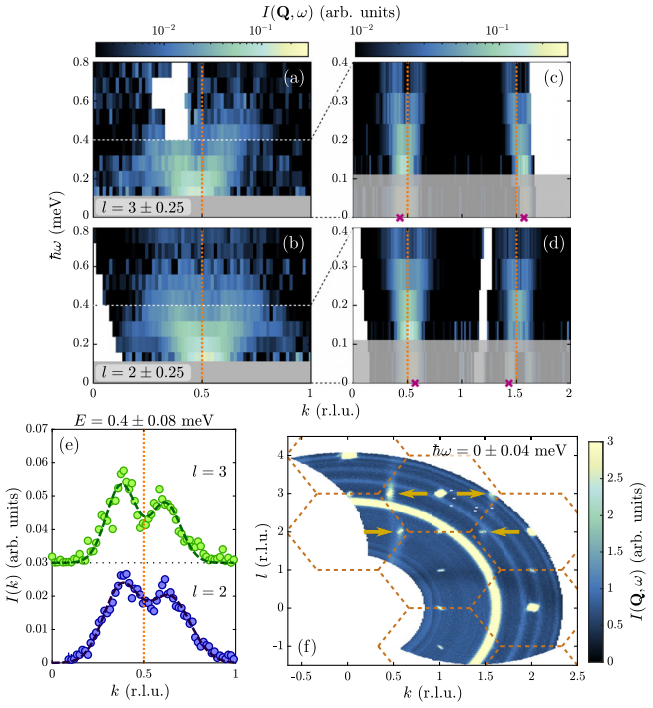

FIG. 4. (a), (b) Low-energy dynamics in the SDW phase of Cs_2CoBr_4 measured at $T \lesssim 0.1$ K and $\mu_0 H = 1.8$ T. The panels show overviews of the "continuum" part at even and odd l with (c), (d) zoom into the lowest accessible energies correspondingly. Magenta crosses mark the positions of the magnetic Bragg peaks, orange dashed lines show the $k = 1/2$ zone centers. The scattering in grayed areas is dominated by the incoherent line. All data are background-subtracted. (e) Intensity-momentum cut at two l values. The energy integration range is shown. Dashed lines are double-Gaussian fit. The $l = 3$ curve is shifted upwards for visibility. (f) $0kl$ plane at $\hbar\omega = 0$ meV. Arrows indicate the positions of SDW Bragg peaks. Orange dashed lines mark the effective "triangular" Brillouin zones. Here the background is not subtracted.

easy-plane Co^{2+} ions in transverse field with the anisotropy constant D given above. To conclude, spectral properties of the SDW state are heavily affected by the 2D J' exchange, but only at quite low energies. The high energy part seems to be a result of the interplay of spin-1/2 chainlike physics and Co^{2+} crystal-field effects. Similar arguments apply to the high-field D and E phases [17]. As said, noncommuting fields admix $|\pm 3/2\rangle$ states to the ground state, making the pseudospin-1/2 model inadequate at finite field. Their gapless nature [17] hints at complex structures, among which are incommensurate planar states or spin-density waves [2].

In conclusion, for the first time we have observed the generation of an incommensurate longitudinal SDW phase and its locking into an UUD magnetization plateau state, driven by quasi-2D correlations in a $J - J'$ distorted triangular lattice magnet. While there may exist some easy-axis anisotropy in both the intra- and interchain

exchange, the frustration of zig-zag bonds appears to be the primary mechanism defining the phase diagram of magnetized Cs_2CoBr_4. This material appears to be an ideal platform for exploring the interplay of anisotropy and frustration. This exotic frustrated physics, interpolating between 1D and 2D worlds, calls for intense future experiments and in-depth theoretical analysis.

We acknowledge the beam time allocation at PSI and ILL (TASP id: 20200145, CAMEA id: 20211018, D23 ID: 5-41-1086). J. L. was supported by the Danish National Committee for Research Infrastructure through DanScatt. We thank Dr. Denis Golosov (Bar Ilan University) for insightful discussions.

*lfacheri@phys.ethz.ch
†zhelud@ethz.ch

[1] T. Giamarchi, *Quantum Physics in One Dimension* (Clarendon Press, Oxford, 2004).
[2] O. A. Starykh, Unusual ordered phases of highly frustrated magnets: A review, Rep. Prog. Phys. **78**, 052502 (2015).
[3] G. Grüner, The dynamics of spin-density waves, Rev. Mod. Phys. **66**, 1 (1994).
[4] F. D. M. Haldane, General Relation of Correlation Exponents and Spectral Properties of One-Dimensional Fermi Systems: Application to the Anisotropic $S = 1/2$ Heisenberg Chain, Phys. Rev. Lett. **45**, 1358 (1980); N. M. Bogoliubov, A. G. Izergin, and V. E. Korepin, Critical exponents for integrable models, Nucl. Phys. **B275**, 687 (1986); T. Hikihara and A. Furusaki, Correlation amplitudes for the spin-$\frac{1}{2}$ XXZ chain in a magnetic field, Phys. Rev. B **69**, 064427 (2004).
[5] K. Okunishi and T. Suzuki, Field-induced incommensurate order for the quasi-one-dimensional *XXZ* model in a magnetic field, Phys. Rev. B **76**, 224411 (2007).
[6] S. Kimura, M. Matsuda, T. Masuda, S. Hondo, K. Kaneko, N. Metoki, M. Hagiwara, T. Takeuchi, K. Okunishi, Z. He, K. Kindo, T. Taniyama, and M. Itoh, Longitudinal Spin Density Wave Order in a Quasi-1D Ising-like Quantum Antiferromagnet, Phys. Rev. Lett. **101**, 207201 (2008).
[7] E. Canévet, B. Grenier, M. Klanjšek, C. Berthier, M. Horvatić, V. Simonet, and P. Lejay, Field-induced magnetic behavior in quasi-one-dimensional Ising-like antiferromagnet $BaCo_2V_2O_8$: A single-crystal neutron diffraction study, Phys. Rev. B **87**, 054408 (2013).
[8] L. Shen, O. Zaharko, J. O. Birk, E. Jellyman, Z. He, and E. Blackburn, Magnetic phase diagram of the quantum spin chain compound $SrCo_2V_2O_8$: A single-crystal neutron diffraction study, New J. Phys. **21**, 073014 (2019).
[9] C. E. Agrapidis, J. van den Brink, and S. Nishimoto, Field-induced incommensurate ordering in Heisenberg chains coupled by Ising interaction: Model for ytterbium aluminum perovskite $YbAlO_3$, Phys. Rev. B **99**, 224423 (2019).
[10] Y. Fan, J. Yang, W. Yu, J. Wu, and R. Yu, Phase diagram and quantum criticality of Heisenberg spin chains with Ising anisotropic interchain couplings, Phys. Rev. Research **2**, 013345 (2020); Y. Fan and R. Yu, Role of the spin anisotropy of the interchain interaction in weakly coupled antiferromagnetic Heisenberg chains, Chin. Phys. B **29**, 057505 (2020).
[11] L. S. Wu, S. E. Nikitin, Z. Wang, W. Zhu, C. D. Batista, A. M. Tsvelik, A. M. Samarakoon, D. A. Tennant, M. Brando, L. Vasylechko, M. Frontzek, A. T. Savici, G. Sala, G. Ehlers, A. D. Christianson, M. D. Lumsden, and A. Podlesnyak, Tomonaga-Luttinger liquid behavior and spinon confinement in $YbAlO_3$, Nat. Commun. **10**, 698 (2019).
[12] S. E. Nikitin, S. Nishimoto, Y. Fan, J. Wu, L. S. Wu, A. S. Sukhanov, M. Brando, N. S. Pavlovskii, J. Xu, L. Vasylechko, R. Yu, and A. Podlesnyak, Multiple fermion scattering in the weakly coupled spin-chain compound $YbAlO_3$, Nat. Commun. **12**, 3599 (2021).
[13] O. A. Starykh, H. Katsura, and L. Balents, Extreme sensitivity of a frustrated quantum magnet: Cs_2CuCl_4, Phys. Rev. B **82**, 014421 (2010).
[14] R. Chen, H. Ju, H.-C. Jiang, O. A. Starykh, and L. Balents, Ground states of spin-$\frac{1}{2}$ triangular antiferromagnets in a magnetic field, Phys. Rev. B **87**, 165123 (2013).
[15] O. A. Starykh and L. Balents, Excitations and quasi-one-dimensionality in field-induced nematic and spin density wave states, Phys. Rev. B **89**, 104407 (2014).
[16] A. V. Chubukov and D. I. Golosov, Quantum theory of an antiferromagnet on a triangular lattice in a magnetic field, J. Phys. Condens. Matter **3**, 69 (1991).
[17] K. Y. Povarov, L. Facheris, S. Velja, D. Blosser, Z. Yan, S. Gvasaliya, and A. Zheludev, Magnetization plateaux cascade in the frustrated quantum antiferromagnet Cs_2CoBr_4, Phys. Rev. Research **2**, 043384 (2020).
[18] R. Coldea, D. A. Tennant, A. M. Tsvelik, and Z. Tylczynski, Experimental Realization of a 2D Fractional Quantum Spin Liquid, Phys. Rev. Lett. **86**, 1335 (2001).
[19] Y. Tokiwa, T. Radu, R. Coldea, H. Wilhelm, Z. Tylczynski, and F. Steglich, Magnetic phase transitions in the two-dimensional frustrated quantum antiferromagnet Cs_2CuCl_4, Phys. Rev. B **73**, 134414 (2006).
[20] T. Ono, H. Tanaka, T. Nakagomi, O. Kolomiyets, H. Mitamura, F. Ishikawa, T. Goto, K. Nakajima, A. Oosawa, Y. Koike, K. Kakurai, J. Klenke, P. Smeibidle, M. Meißner, and H. A. Katori, Phase transitions and disorder effects in pure and doped frustrated quantum antiferromagnet Cs_2CuBr_4, J. Phys. Soc. Jpn. **74S**, 135 (2005).
[21] M. Kenzelmann, R. Coldea, D. A. Tennant, D. Visser, M. Hofmann, P. Smeibidl, and Z. Tylczynski, Order-to-disorder transition in the *XY*-like quantum magnet Cs_2CoCl_4 induced by noncommuting applied fields, Phys. Rev. B **65**, 144432 (2002).
[22] O. Breunig, M. Garst, E. Sela, B. Buldmann, P. Becker, L. Bohatý, R. Müller, and T. Lorenz, Spin-$\frac{1}{2}$ *XXZ* Chain System Cs_2CoCl_4 in a Transverse Magnetic Field, Phys. Rev. Lett. **111**, 187202 (2013); O. Breunig, M. Garst, A. Rosch, E. Sela, B. Buldmann, P. Becker, L. Bohatý, R. Müller, and T. Lorenz, Low-temperature ordered phases of the spin-$\frac{1}{2}$ XXZ chain system Cs_2CoCl_4, Phys. Rev. B **91**, 024423 (2015).
[23] P. Laurell, A. Scheie, C. J. Mukherjee, M. M. Koza, M. Enderle, Z. Tylczynski, S. Okamoto, R. Coldea, D. A. Tennant, and G. Alvarez, Quantifying and Controlling

Entanglement in the Quantum Magnet Cs_2CoCl_4, Phys. Rev. Lett. **127**, 037201 (2021).
[24] M. E. Lines, Magnetic properties of $CoCl_2$ and $NiCl_2$, Phys. Rev. **131**, 546 (1963).
[25] G. Jackeli and G. Khaliullin, Mott Insulators in the Strong Spin-Orbit Coupling Limit: From Heisenberg to a Quantum Compass and Kitaev Models, Phys. Rev. Lett. **102**, 017205 (2009).
[26] S. P. Gosuly, Neutron scattering studies of low-dimensional quantum spin systems, Ph.D. thesis, University College London, 2016.
[27] A. S. Wills, A new protocol for the determination of magnetic structures using simulated annealing and representational analysis (SARA*h*), Physica (Amsterdam) **276B**, 680 (2000).
[28] See Supplemental Material at http://link.aps.org/supplemental/10.1103/PhysRevLett.129.087201 for detailed discussion of the neutron diffraction and inelastic data analysis, Hamiltonian parameter estimates, and the details of the spectra.
[29] J. Rodríguez-Carvajal, Recent advances in magnetic structure determination by neutron powder diffraction, Physica (Amsterdam) **192B**, 55 (1993).
[30] M. Markó, F. Groitl, J. O. Birk, P. G. Freeman, K. Lefmann, N. B. Christensen, C. Niedermayer, F. Jurányi, J. Lass, A. Hansen, and H. M. Rønnow, Prototype of the novel CAMEA concept—A backend for neutron spectrometers, Rev. Sci. Instrum. **89**, 015105 (2018); J. Lass, H. Jacobsen, D. G. Mazzone, and K. Lefmann, MJOLNIR: A software package for multiplexing neutron spectrometers, SoftwareX **12**, 100600 (2020).
[31] S. Toth and B. Lake, Linear spin wave theory for single-Q incommensurate magnetic structures, J. Phys. Condens. Matter **27**, 166002 (2015).
[32] R. Coldea, D. A. Tennant, and Z. Tylczynski, Extended scattering continua characteristic of spin fractionalization in the two-dimensional frustrated quantum magnet Cs_2CuCl_4 observed by neutron scattering, Phys. Rev. B **68**, 134424 (2003).
[33] D. A. Tennant, S. E. Nagler, D. Welz, G. Shirane, and K. Yamada, Effects of coupling between chains on the magnetic excitation spectrum of $KCuF_3$, Phys. Rev. B **52**, 13381 (1995).
[34] J. Jensen and A. R. Mackintosh, *Rare Earth Magnetism: Structures and Excitations*, International Series of Monographs on Physics (Clarendon Press, Oxford, 1991).
[35] M. Kohno, O. A. Starykh, and L. Balents, Spinons and triplons in spatially anisotropic frustrated antiferromagnets, Nat. Phys. **3**, 790 (2007).
[36] H. Shiba, Quantization of magnetic excitation continuum due to interchain coupling in nearly one-dimensional Ising-like antiferromagnets, Prog. Theor. Phys. **64**, 466 (1980).
[37] B. Grenier, S. Petit, V. Simonet, E. Canévet, L.-P. Regnault, S. Raymond, B. Canals, C. Berthier, and P. Lejay, Longitudinal and Transverse Zeeman Ladders in the Ising-Like Chain Antiferromagnet $BaCo_2V_2O_8$, Phys. Rev. Lett. **114**, 017201 (2015).